Building a Practical Natural Laminar Flow Design Capability

Richard L. Campbell [1] and Michelle N. Lynde [2]
NASA Langley Research Center, Hampton, Virginia, 23681

A preliminary natural laminar flow (NLF) design method that has been developed and applied to supersonic and transonic wings with moderate-to-high leading-edge sweeps at flight Reynolds numbers is further extended and evaluated in this paper. The modular design approach uses a knowledge-based design module linked with different flow solvers and boundary layer stability analysis methods to provide a multifidelity capability for NLF analysis and design. An assessment of the effects of different options for stability analysis is included using pressures and geometry from an NLF wing designed for the Common Research Model (CRM). Several extensions to the design module are described, including multiple new approaches to design for controlling attachment line contamination and transition. Finally, a modification to the NLF design algorithm that allows independent control of Tollmien-Schlichting (TS) and cross flow (CF) modes is proposed. A preliminary evaluation of the TS-only option applied to the design of an NLF nacelle for the CRM is performed that includes the use of a low-fidelity stability analysis directly in the design module.

Nomenclature

AL	=	Attachment line
BLSTA3D	=	Boundary Layer code for Stability Analysis 3D, boundary layer profile solver
c	=	Chord length
CART3D	=	Cartesian 3D, Euler flow solver
CDISC	=	Constrained Direct Iterative Surface Curvature, design module
CF	=	Cross flow
c_l	=	Sectional lift coefficient
c_m	=	Sectional pitching moment coefficient
C_P	=	Pressure coefficient
CRM	=	Common Research Model
LASTRAC	=	Langley Stability and Transition Analysis Code, transition prediction software
LFC	=	Laminar flow control
LST	=	Linear stability theory
MATTC	=	Modal Amplitude Tracking and Transition Computation, transition prediction software
NASA	=	National Aeronautics and Space Administration
NF	=	N-factor
NLF	=	Natural laminar flow
NTF	=	National Transonic Facility
OTS	=	Oblique Tollmien-Schlichting
Re_Θ	=	Reynolds number based on attachment line boundary layer momentum thickness
Re_c	=	Reynolds number based on local chord length
Re_T	=	Reynolds number based on chordwise transition location
rle	=	Leading-edge radius
TCF	=	Traveling cross flow
TetrUSS	=	Tetrahedral Unstructured Software System, flow solver package
TS	=	Tollmien-Schlichting

[1] Senior Research Engineer, Configuration Aerodynamics Branch, NASA Langley Research Center M/S 499 Hampton, VA 23681, AIAA Associate Fellow.
[2] Research Aerospace Engineer, Configuration Aerodynamics Branch, NASA Langley Research Center M/S 499 Hampton, VA 23681, AIAA Member.

UDF = Universal damping function, CDISC NLF design parameter
USM3D = Unstructured Mesh 3D, Navier-Stokes flow solver
VGRID = Unstructured grid generator
x/c = x-location nondimensionalized by local chord
y = Semispan location
β = Wave number
γ = ratio of specific heats, 1.4 for air
Λ_{LE} = Leading-edge sweep

I. Introduction

NATURAL laminar flow (NLF) is a technology that has been recognized for decades as having the potential to reduce aircraft drag and thus both fuel burn and emissions. Though primarily seen only on experimental and recreational aircraft in the past, it is now finding its way onto commercial aircraft for selected components with either low sweep or low Reynolds number such as nacelles, winglets and business jet wings[1,2]. The reason for its limited application thus far is that NLF, while more desirable than laminar flow control (LFC) because of its simplicity, at least historically has required a reduction in wing sweep with increasing Reynolds number to control the cross flow (CF) mode of transition. A notional representation of the current NLF-LFC boundary is shown by the blue line in figures 1a and 1b. Figure 1a includes our rough estimates of the sweeps and transition Reynolds numbers for the components with NLF mentioned above on aircraft currently in service. In previous papers[3,4], we described the initial development of an NLF design approach that could expand the boundary of NLF in terms of both sweep and Reynolds number and gave a couple of preliminary illustrations of its application to transonic and supersonic commercial transports (Figure 1b).

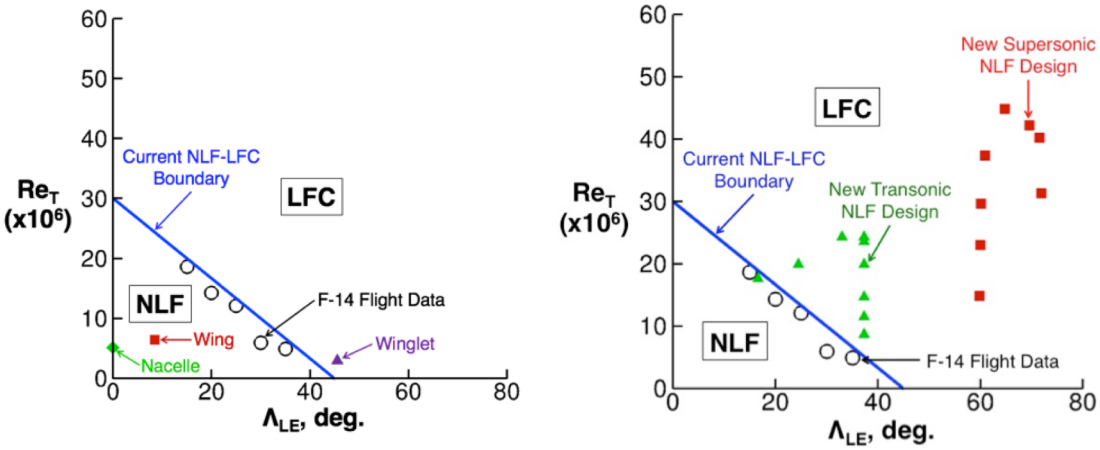

a) NLF technology currently in service. **b) NLF design approach results.**

Figure 1. New designs relative to current NLF-LFC boundary in terms of leading-edge sweep (Λ_{LE}) and transition Reynolds number (Re_T).

In a companion paper entitled "Computational Design and Analysis of a Transonic Natural Laminar Flow Wing for a Wind Tunnel Model", we discuss the application of this current method to the design of an NLF wing for a semi-span model based on the Common Research Model (CRM)[5] for testing in the National Transonic Facility (NTF) at the NASA Langley Research Center. The purpose of the proposed test would be two-fold: 1) validate the new NLF design methodology; and 2) evaluate NLF testing for semispan wings in the NTF in light of some recent and proposed improvements to the tunnel as well as testing processes. This second paper gives detailed results from the design, including off-design assessments, as well as describing a testing approach for isolating various modes of transition, a distinction that is needed for tunnel characterization.

In the current paper, we will discuss some of the questions and issues that came up as we did the above design, but also as we began to incorporate our initial method into a practical NLF design capability and apply it to other configurations and components. This will include consideration of additional flow and geometry constraints, as well as evaluations of some of the assumptions used in our processes – in particular, our approach to computing transition locations. Recommendations of best practices to date will be made when possible. This paper will follow the outline given below.

First, a general description of the computation methods used in the design process will be given. Following that, our approach for addressing each of the primary types of transition considered (attachment line contamination/transition (AL), cross flow (CF), and Tollmien-Schlichting (TS)) will be described. This will include a description of the CDISC constraints used to control each transition mechanism as well as the stability analysis used in each case, along with an assessment of some alternative ways of computing N-factor (NF) growth for estimating transition location. Finally, we will describe some overall design process considerations for improving the efficiency, accuracy and robustness of the method.

II. Methods

Our general approach to NLF analysis and design can be seen in the flow chart in Figure 2. The modular nature of the process allows the use of different levels of fidelity in both the flow solver and stability analysis, with converter codes (not shown) used to account for differences in the input/output formats for each code. The transition prediction and design loops are independent of each other and typically are called at different frequencies. Further discussion on this is included in the process section at the end of the paper. For the studies included in this paper, two flow solvers and two transition prediction methods were used, each reflecting different levels of flow physics modeling.

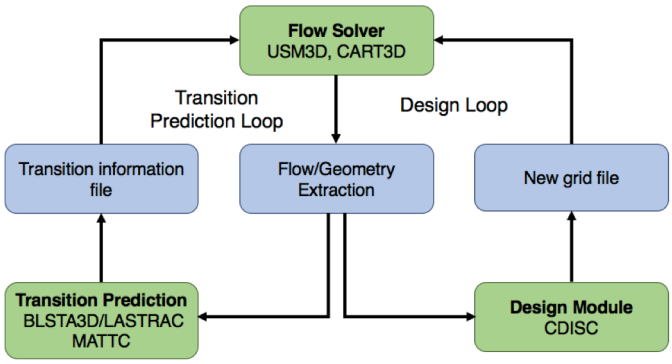

Figure 2. Flow chart of the NLF analysis and design process.

A. Flow Solvers

Our primary flow solver was the USM3D code, part of the TetrUSS software system[6]. This code solves the Navier-Stokes equations on an unstructured, tetrahedral-cell grid. For our cases, the grids were generated using the VGRID code within TetrUSS framework using typical practices for turbulent flow cases, but with finer chordwise surface grid resolution prescribed at the leading edge to resolve the steep flow gradients used in our NLF design process. As we used an external boundary layer solver to provide the profiles for the stability analysis, we did not need to utilize additional viscous layers in the grid, retaining our standard practice of about 30 layers, with the first point off of the surface having a value of y+ of 0.5. The grids are typically on the order of 30-40 million grid cells, depending on what aircraft components are present. The flow solution is performed on the grid using a cell-centered, upwind formulation and no limiter was invoked. For all of our cases, the Spalart-Allmaras turbulence model was used in regions with turbulent flow and the forced-laminarization option was used ahead of the predicted transition front. One helpful feature of USM3D is the ability to prescribe an arbitrary transition front, as opposed to having to follow structured grid lines on the surface.

While USM3D is our primary flow solver for cases such as transonic wing designs where viscous effects are important and more exact drag estimates are required, there are times where the very efficient inviscid CART3D flow solver[7] is a good choice, especially in exploring new design approaches or configurations. This flow solver was used effectively in our previous supersonic NLF wing design where viscous effects were small and will be applied to an NLF nacelle design described later in this paper. CART3D solves the Euler equations on a Cartesian mesh that is automatically generated around a triangulated surface definition. There are options available for adjoint-based design and grid adaption, although these were not used in the current study. However, a prescribed local refinement option was used to give better resolution of the flow near the lip of the nacelle. To obtain the surface triangulation used in CART3D, we typically just extract the surface grid from the full USM3D grid and write it in the required format.

B. Transition Prediction

Our primary stability analysis tool is the LASTRAC software[8], which provides a variety of analysis levels ranging from linear stability theory (LST) to linear and nonlinear parabolized stability equations (PSE and NPSE, respectively). Included in these levels are several other options such as compressibility and curvature effects. In our designs to date, both transonic and supersonic, we have used LST computations that included compressibility but not

curvature effects. We have also assumed that, for transonic flow, the dominant modes are freestream TS with wave number (β) set to zero, and stationary CF with frequency set to zero. For supersonic wing design, with local Mach numbers well above 1.5, we include nonzero frequency-β pairs to assess both oblique TS (OTS) and traveling CF (TCF) modes. In addition, we have used a fixed-β approach as opposed to an envelope method[9] and have performed the computations along a streamwise cut through the wing instead of along a streamline. Results from a brief look at the validity of some of those assumptions are included in the Results section.

The LASTRAC computation requires boundary layer profiles based on the flow solution. We utilize the BLSTA3D boundary layer code to provide these profiles based on either the target or analysis pressure coefficient (C_P) distributions and the airfoil section geometries used in the design process. BLSTA3D has options for computing the profiles based on an infinite swept wing or for conical flow, simulating both wing sweep and taper[10]. The conical flow option was selected as our wing geometry is generally conical, though the flow isobars are not fully consistent with this assumption, tending to be more streamwise (see figure 3). The authors have developed a version of BLSTA3D that attempts to use local isobar sweep values and are investigating its application to these atypical NLF wing isobar patterns. Some attempts were also made to compare results from BLSTA3D profiles with ones extracted directly from the USM3D flow solution. Preliminary results indicated good agreement for the profiles themselves, but inconsistencies in the LASTRAC output precluded the inclusion of those results in this paper. In addition to the profiles, the BLSTA3D code provides the values of momentum thickness Reynolds number, Re_Θ, used in the attachment line state assessments.

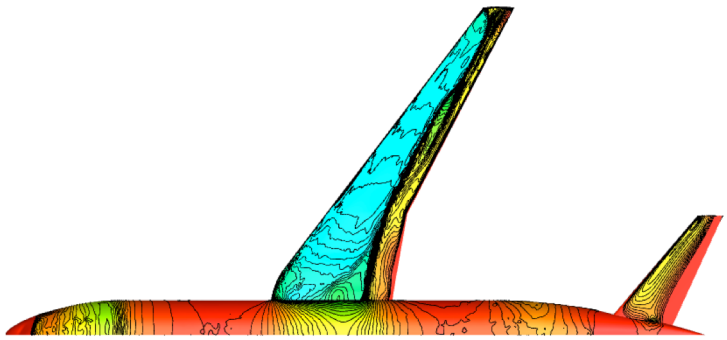

Figure 3. Isobar plot of a NLF wing design.

As mentioned earlier, the LASTRAC computation has not been included in the design loop, primarily because of the cost. The time required for a single LST analysis run for a transonic wing with 10-15 design stations and only free-stream TS and stationary CF modes considered can easily be the same as 10 cycles through the design loop. As an alternative, the MATTC method has been shown to provide reasonable estimates of transition location in 2-3 orders of magnitude less time. The code uses semiempirical functions whose coefficients can be calibrated based on LASTRAC results for the baseline or initial target pressure distributions for improved accuracy[11]. In addition, a new feature has been added to MATTC to predict leading edge CF peak heights as the original version did not predict CF growth well for our NLF pressure distributions. Evaluations of the codes capability versus LASTRAC results are included in the Results section.

C. Design Module

The design module used in our process is the CDISC knowledge-based design method[12]. It uses prescribed sensitivity derivatives to determine the geometry changes needed to match a flow target, typically a target pressure distribution. This approach is well-suited for the NLF design problem where the pressures are a main driver relative to N-factor growth. Also, the elimination of the need to compute the sensitivity derivatives greatly reduces the computational time relative to other design methods such as numerical optimization. Flow constraint options within CDISC are used to define the target pressures by modifying the current analysis pressures to meet specified flow characteristics such as section lift or pitching moment. For NLF design, the pressure levels and gradients are adjusted to provide a given extent of laminar flow while also meeting the two aforementioned characteristics.

The CDISC design algorithm will attempt to match the target pressure distribution subject to geometry constraints. Two important geometry constraints used in NLF designs are leading-edge radius and local surface curvature. The radius is specified to help meet the criteria for avoiding attachment line contamination and transition as well as helping to match the target pressures near the leading edge of the airfoil. The curvature constraint is set to prevent a concave surface in the laminar region in order to avoid transition due to Görtler vortices. A thickness constraint is also used to maintain the original airfoil maximum thickness at each design station. Several modifications to existing constraints to help address NLF issues will be described in the following section.

III. Results

This section highlights some of the questions that we attempted to answer in moving toward a validated design process. Each subsection will address one of the primary modes of transition and include issues related to flow analysis, transition prediction and/or design. An additional mode of transition, Görtler vortices, was addressed by limiting wing upper surface curvatures to convex-only and is not discussed below. In the final subsection, some observations on the design process itself and best practices to date will be included.

A. Attachment Line Contamination and Transition

A turbulent attachment line (AL) on the wing leads to a global collapse failure mode where the loss of laminar flow is full-chord and full-span unless the attachment line is relaminarized further outboard. Past research by Poll[13] has led to correlations with the momentum thickness Reynolds number (Re_Θ) at the wing leading edge for attachment line contamination and transition. If Re_Θ can be reduced below 100 for a distance of approximately 50 boundary layer heights, turbulence cannot be maintained and a turbulent attachment line running onto the wing from the fuselage will return to a laminar state. As long as the attachment line Re_Θ outboard of this location is kept below 235, the attachment line will remain in a laminar state on a smooth leading edge (e.g., no bugs or ice).

The equation below is Poll's estimate of the Re_Θ parameter based on flow about an infinite swept cylinder, modified to use the leading-edge radius (rle) measured in the streamwise direction and nondimensionalized by local wing chord to be consistent with the CDISC geometry constraint.

$$Re_\Theta = 0.404^* \{Re_c * rle * \tan(\Lambda)\}^{0.5} \quad (1)$$

In this equation, Re_c is the Reynolds number base on local chord and Λ is the sweep of the wing leading edge. For wings with low sweep or low Reynolds number, keeping Re_Θ below 100 is typically not an issue. For example, at a sweep of 20 degrees and a chord Reynolds number of 20 million, the value of rle would have to remain below 0.0084. The airfoils on the CRM model, typical of a modern transport, have rle values below this value across nearly the entire wing.

In our previous reports, we assessed the state of the attachment line, noting where the two constraints (contamination and transition) were violated, but did not attempt to change the flow. When the wing design involves higher values of sweep or Reynolds number, several approaches can be taken to avoid attachment line contamination. Previously researchers have proposed and tested devices such as bumps[14,15] and slots[16] to divert the turbulent attachment line off the leading edge and downstream over the wing, creating a new laminar attachment line just outboard of the device. In this paper, we evaluate two new CDISC constraints that adjust the leading-edge radius or sweep of the wing near the root, attempting to relaminarize the attachment line rather than divert it. Examples of the applications of these constraints to the CRM model are given below.

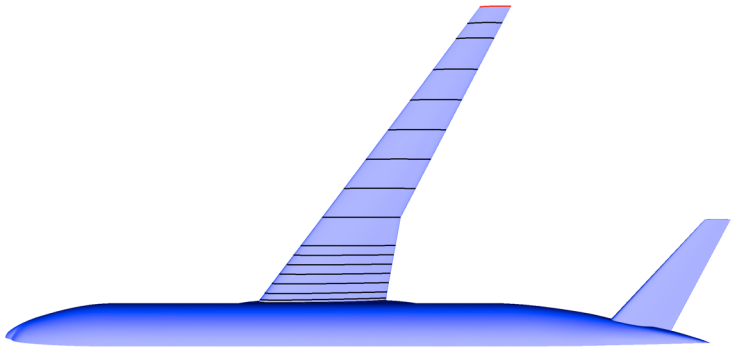

Figure 4. Planform view of CRM with wing design stations shown as black lines.

The baseline CRM wing has a leading-edge sweep of 37.3 degrees and a Reynolds number based on mean aerodynamic chord of 30 million for these cases. Figure 4 shows a planform view of the configuration with the stations used for analysis and design indicated by black streamwise lines on the wing. A plot of the Re_Θ values across the span for the baseline (figure 5) shows that they are below the 235 limit except at the wing root, so that relaminarizing the attachment line inboard should allow it to remain laminar outboard. A boundary layer profile was extracted from the flow solution in the attachment line near the wing root. Analysis of this profile gave an estimate of the boundary layer thickness of about 0.05, giving a

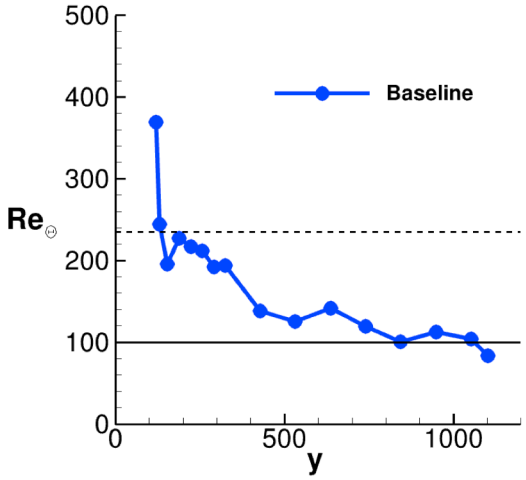

Figure 5. Spanwise distribution of Re_Θ for the baseline CRM configuration (y in inches).

required distance of Re_Θ values below 100 of 50 x 0.05 = 2.5 inches (full scale). To be conservative, the Re_Θ will be required to stay below 100 at design stations 2 and 3, or a distance of 35 inches.

The first approach aims to relaminarize the attachment line by reducing leading-edge radius. This approach uses an existing CDISC leading-edge radius constraint, LERAD. Figure 6 shows the Re_Θ values for the first 5 design stations on the wing outboard of the fuselage juncture, with the baseline values in blue. The application of the radius constraint with rle values based on Eq. 1 are shown in red and indicate little reduction in Re_Θ. The reason for this is that the attachment line for the inboard airfoils at these lift conditions is not located at the leading edge where the curvature has been reduced (see figure 7). As we noted in Lynde[4], reducing the radius at the leading edge of an airfoil will generally increase the local radius of curvature just aft of it, possibly where the attachment line is located. To counter this effect, a new option was added to the CDISC flap constraint (FLAP) to adjust the deflection of the leading edge to locate the attachment line closer to x/c = 0. The results from a preliminary application of this constraint using a 0.25c smooth variable camber leading-edge flap are shown as the green line in figure 6. The Re_Θ values are all very close to the 100 limit and provide a confirmation of using Eq. 1, although it appears that some additional radius reduction would be needed to provide a conservative design. It should also be noted that, while drooping the leading edge is helpful in meeting the attachment line criteria, it may be detrimental relative to achieving the steep pressure gradient required at the leading edge to control CF growth.

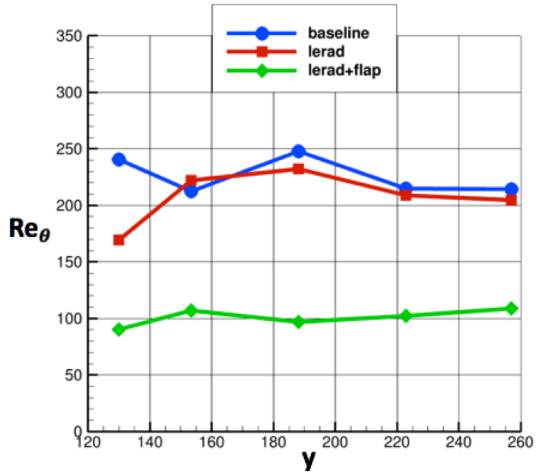

Figure 6. Attachment line Re_Θ results for LERAD and LERAD+FLAP designs (y in inches).

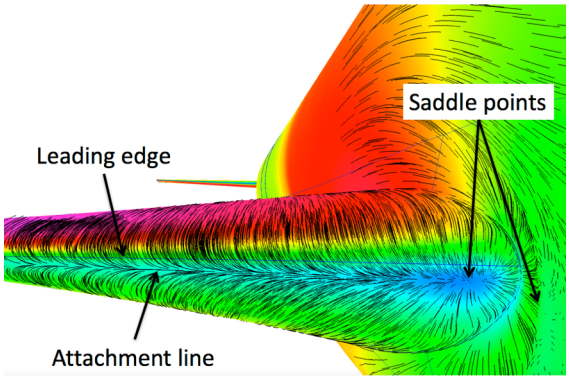

Figure 7. Inboard wing attachment line location for CRM baseline.

Another observation regarding figure 7 is that there is a separation region where the wing leading edge joins the fuselage, creating the 2 "saddle points" labeled in the figure. For the saddle point on the wing, the flow near the surface inboard of the point is moving toward the fuselage, then forward toward the 2nd saddle point on the fuselage. Often a fillet or "horn" is placed in this area to eliminate the saddle points and weaken the horseshoe vortex around the wing-fuselage juncture. It is not clear to the authors if the presence of the saddle point on the wing is an indication of the beginning of a new laminar boundary layer at the attachment line or if the fuselage boundary layer can somehow bridge the separation zone and still impact the wing. If the former is true, then no further device or treatment would be needed to avoid attachment line contamination, though attachment line transition would still need to be addressed.

The second approach to controlling attachment line contamination aims to relaminarize the attachment line by reducing leading-edge sweep. This approach uses a new CDISC constraint, LEMOD, to alter the planform of the wing near the root. The magnitude of the sweep change is driven by Re_Θ results from the BLSTA3D code updated during each design cycle. The Re_Θ results for the final design are shown in figure 8, with the baseline and final design planforms shown in figure 9. This design approach as well as the first one using the LERAD and FLAP constraints appear to be feasible approaches to relaminarizing the attachment line, with both approaches possibly requiring a lower target Re_Θ to ensure a conservative design. The LEMOD approach had a stronger effect at the root in reducing Re_θ and was thought to be somewhat more robust in that the other approach had the flap angle tuned to the cruise condition. The LEMOD planform does have a slight (< 1%) reduction in wing area and may tend to strengthen the horseshoe vortex, which could increase drag. Full designs using each method would be needed to give the best comparison of the approaches, but in the interest of provided the best chance of avoiding attachment line contamination for the CRM NLF wind tunnel model, the LEMOD approach was selected for the design.

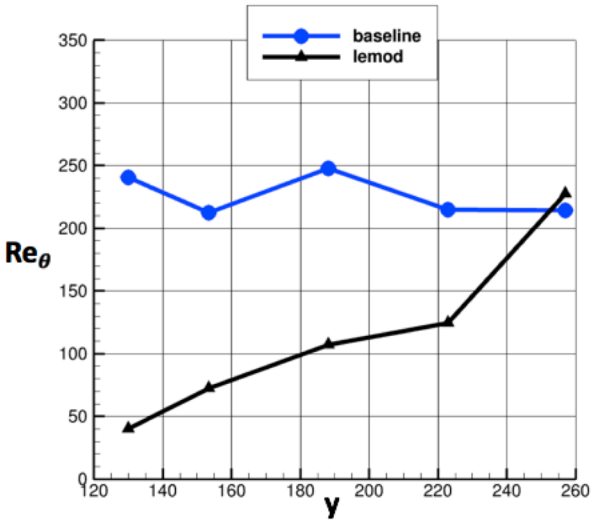

Figure 8. Results for LEMOD design (y in inches).

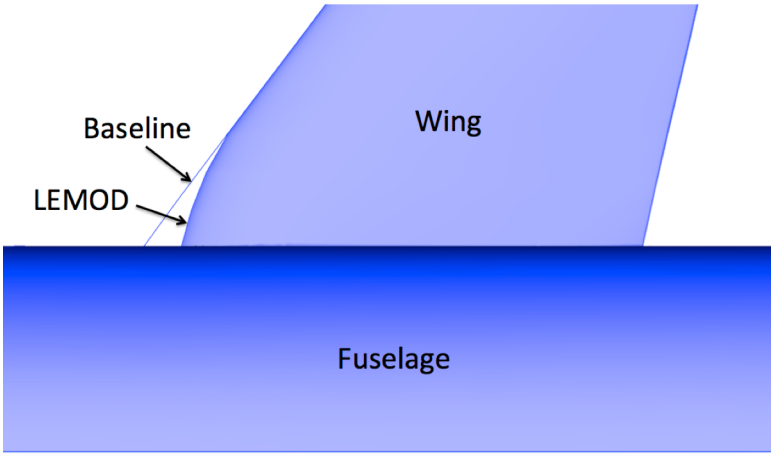

Figure 9. Planform change for LEMOD design.

B. Cross Flow

Once a laminar attachment line is achieved, the next most important mode in terms of extent of natural laminar flow is cross flow. For the range of wing sweeps and Reynolds numbers that we are considering, this mode tends to produce a local collapse failure mode, with a CF peak near the leading edge having the potential to produce nearly full-chord turbulent flow at and between the design stations where the CF N-factor limit is exceeded. The CDISC NLF design constraint, SSNLF, addresses this mode by creating a target pressure with a rapid drop in C_P from the leading edge to X1, followed by a short zero-pressure gradient region from X1 to X2 (see figure 10). The SSNLF constraint seemed to address this mode fairly well, but the designs seldom drive the attachment line to the leading edge as specified in the target pressure. This gave overly optimistic estimates of CF peak reduction, so the target pressures now prescribe the initial acceleration from the leading edge to X1 and use the existing lower surface pressures from the attachment line to the leading edge.

Other questions have arisen as to the best approach to computing the N-factor growth characteristics. In the work to date, the authors have used linear stability theory (LST) with compressibility effects included. In order to investigate

the effects of some of the other options in LASTRAC for computing the N-factor growth curves, the pressure distribution and geometry from design station 6 on the inboard part of the CRM NLF wing will be used (see figure 11). The freestream Mach number is 0.85, Reynolds number based on local chord is 39.8 million, and the leading- and trailing-edge sweep angles are 37.3 and 10.0 degrees, respectively.

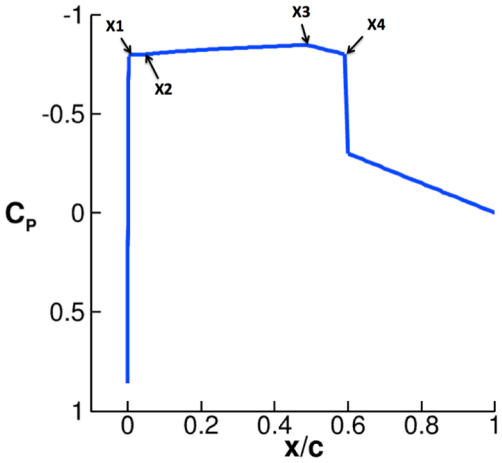

Figure 10. SSNLF pressure architecture.

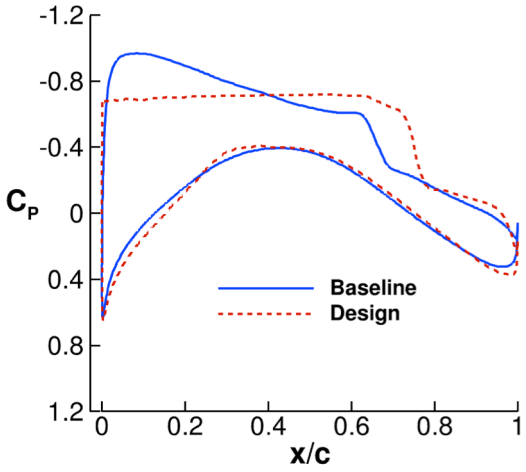

Figure 11. Pressure distribution for baseline and design at station 6.

The effectiveness of the design approach at this design station in controlling the leading-edge CF peak is illustrated in figure 12, with the rapid N-factor growth quickly exceeding the critical N-factor of 10 for the baseline (figure 12a). In figure 12b, it can be seen that the design pressures successfully limit the CF peak to an N-factor level of 8.

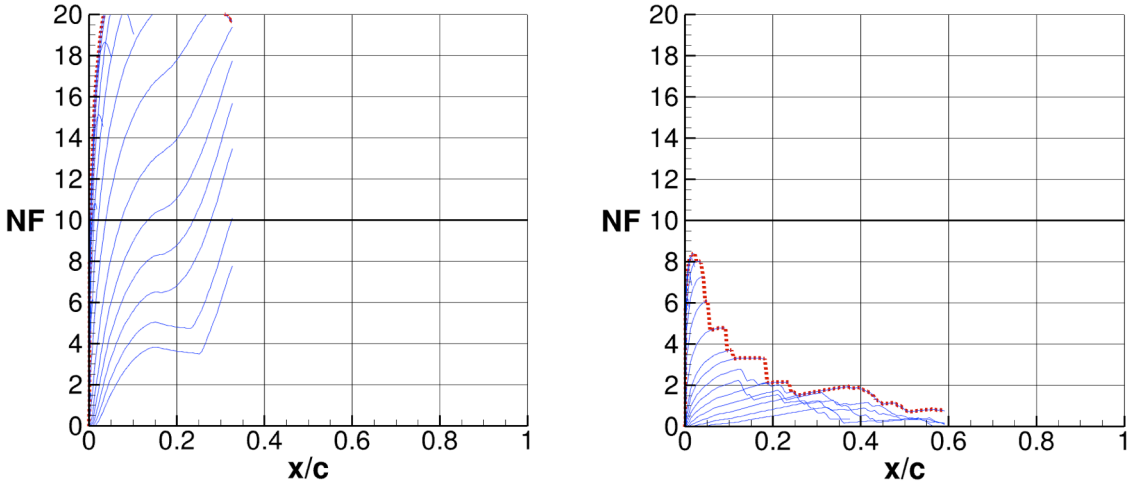

a) Baseline. **b) Design.**

Figure 12. Comparison of CF N-factors for baseline and design at station 6.

While the LASTRAC method does not include an explicit incompressible option, the effect can be simulated by increasing the value of γ by a factor of ten thousand so that the speed of sound is increased, thus reducing the Mach number below 0.01. Comparing figures 13a and 13b shows that the effect of compressibility on the CF N-factor growth is minimal at this Mach number.

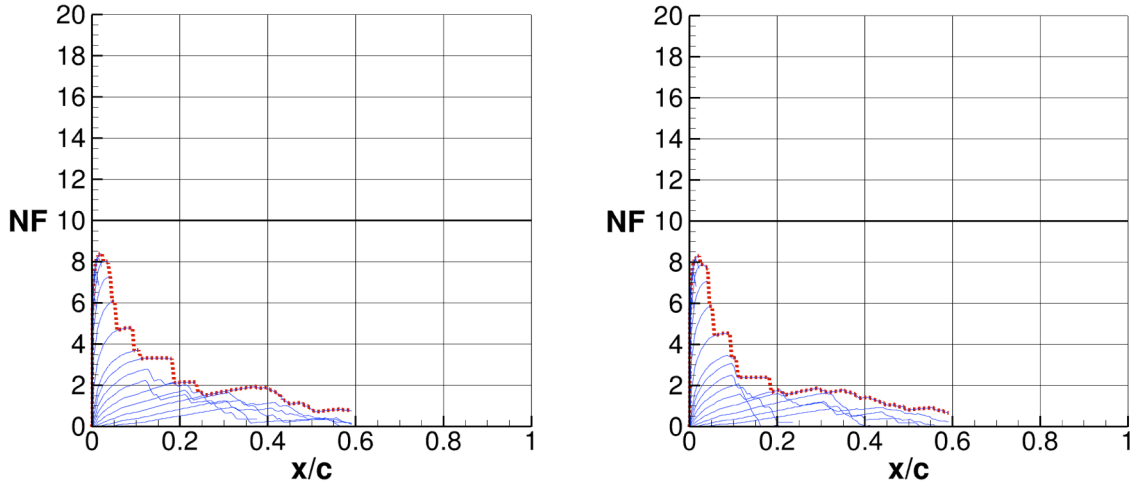

Figure 13. Effect of incompressibility of CF N-factors for design at station 6.

The LASTRAC code does have direct options for including streamwise and traverse (spanwise) curvature effects. As most transport wings have minimal traverse curvature, we only examine the streamwise option. The effect of including streamwise curvature can be seen be comparing figure 14b with 14a. There is a very significant suppression of the CF N-factors in general, including a reduction in the N-factor peak from about 8 to 2. As the largest CF growth occurs near the leading edge where the curvature is the highest, this result is not unexpected. The curvature option essentially adds no time to the computation and, in theory, offers a more accurate estimate of N-factor growth; however, if the critical N-factor level was determined from experimental data without using curvature effects, the inclusion of them could give a false indication of avoiding CF transition.

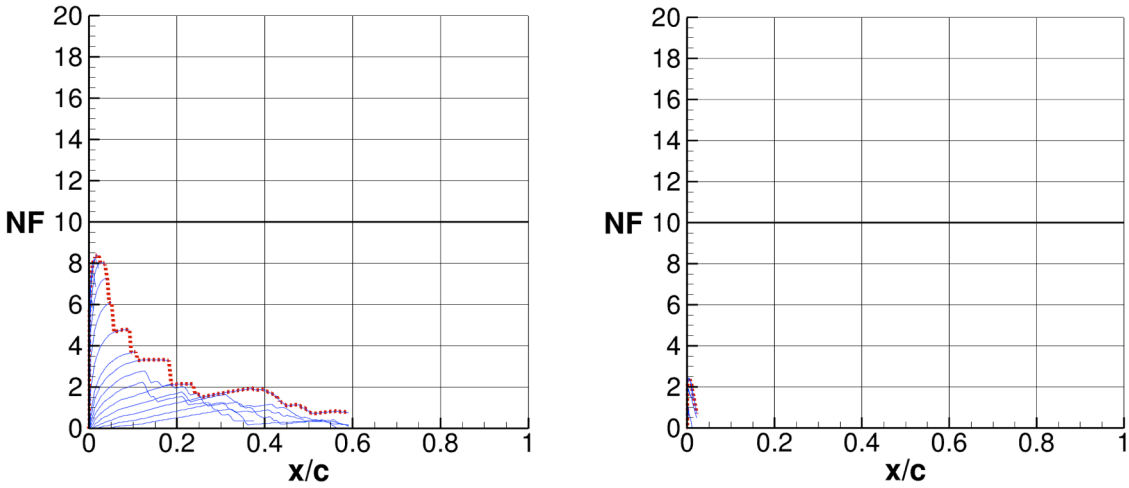

Figure 14. Effect of streamwise curvature of CF N-factors for design at station 6.

As mentioned earlier, our design process has only addressed the stationary form of CF ($\beta = 0$). An assessment of traveling cross flow (TCF) will be included in the next subsection as part of the discussion on using nonzero frequency-β pairs to compute TCF as well as oblique TS waves. One comment for now, however, is that the TCF computations are still performed using the LST level of physics modeling, with the only increase in time coming from the expanded search matrix. In Malik[17], it is noted that it is often the case that curvature effects tend to cancel out the effects of using the PSE higher-fidelity computation so that the resulting N-factor curves from using PSE with curvature would be

similar to LST with no curvature. In figures 15 and 16, we examine first the effect of using PSE versus LST without curvature, and then the impact of curvature on the PSE results. Comparing figure 15b to 15a, it can be seen that, while there is a more extensive region of higher N-factors for the PSE analysis, the peak is only slightly higher than the LST results. When curvature effects are included (figure 16b), the peak height is dramatically reduced to a level similar to that seen in the LST with curvature results (figure 14b). It is not clear why these results are different from the guidance suggested in Malik[17]. Perhaps the atypical pressure architecture used to control CF, as well as the smaller leading-edge radius to avoid AL issues, causes this case to be outside of the range of parameters used to develop the previous understanding. In any case, the significantly higher cost (~30x) of the PSE analysis for CF would probably prohibit it from being used in a practical design process, except perhaps as a final check on the design. Here again, the issue of how the critical N-factor was determined would have to be considered.

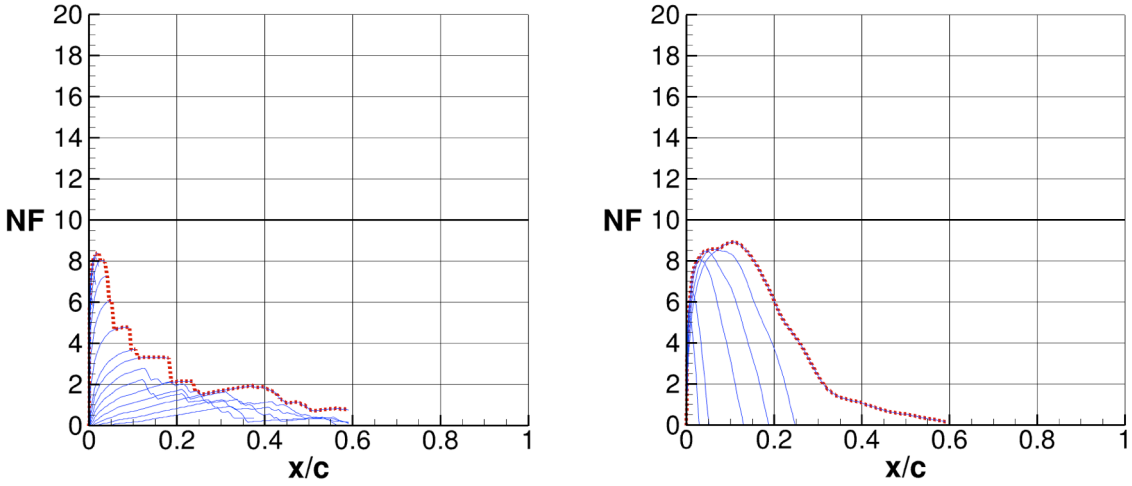

a) LST. b) PSE.

Figure 15. Effect of higher-fidelity analysis on CF N-factors for design at station 6.

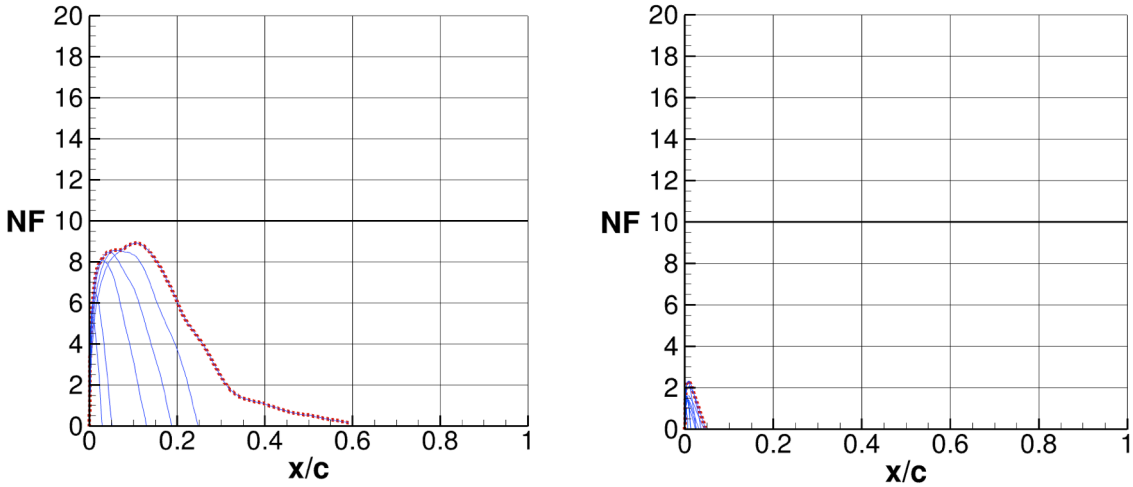

a) No curvature. b) Curvature.

Figure 16. Effect of curvature on higher-fidelity CF N-factors for design at station 6.

The lowest fidelity option available in LASTRAC for stability analysis is LST, but even this is not very amenable to use directly in the design loop, i.e., called at the same frequency as CDISC. For a normal case set-up, one pass through LASTRAC for TS and CF for the upper surface only at each design station typically takes just under an hour for transonic NLF designs and between 4 and 5 hours for a supersonic case. The MATTC method is at least 3 orders of magnitude faster than LASTRAC, but typically requires calibration to produce results that are sufficiently close to

the LST ones. Historically, the CF predictions from MATTC were the least accurate, even with calibration, and the initial attempts at matching the CF growth for our leading-edge pressure architectures confirmed that it is still not adequate.

Noting that our pressure architecture creates a CF peak near the leading edge with decaying values aft of that, an alternate option was created in MATTC to at least predict the peak height. The algorithm used is essentially a reverse application of the one used to prescribe the target pressures from the leading edge to X1; i.e., extract an effective X1 value for the current analysis pressures. Peak CF N-factors computed for the CRM NLF using this new MATTC option are compared with results from LASTRAC LST computations in figure 17a. A reasonable agreement can be seen across the wing, with the MATTC giving slightly higher values near mid semispan, which is a conservative result from a design perspective. As a check on the generality of the algorithm, it was also applied to the supersonic design from our previous work (figure 17b). Here again, the agreement with LASTRAC is fairly good, indicating that it may be a good tool to use during design, with the final flow results confirmed using LASTRAC.

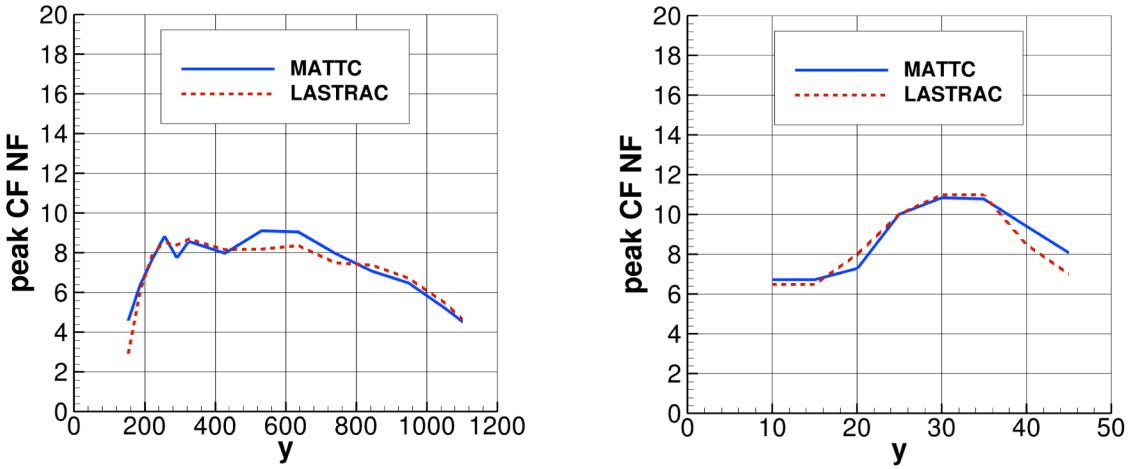

a) Transonic CRM NLF design. **b) Supersonic NLF design.**

Figure 17. Comparison of peak CF N-factors computed using LASTRAC and MATTC (y in inches).

C. Tollmien-Schlichting

The Tollmien-Schlichting (TS) mode of transition is the least catastrophic of the 3 primary modes that our method addresses, typically producing a transition front in the midchord region for an NLF design. As with CF, the existing SSNLF constraint does a reasonable job of controlling TS N-factor growth, typically crossing the critical N-factor level near the desired location. This is accomplished by prescribing the universal damping function (UDF) coefficient based on Reynolds number and critical N-factor between X2 and X3 as shown on figure 10. In earlier versions of the SSNLF constraint, X3 also represented the shock location in transonic target pressures. It was observed that, while pressure levels were often matched fairly well, the target shock location was not always obtained, especially when upper surface curvature constraints were included to give better off-design performance. As a result, the section lift coefficient at the design station was not matched, requiring a change in the configuration angle of attack to match overall lift.

In the new version of SSNLF, the shock location (X4) has been decoupled from the desired transition location (X3) as shown in figure 10. This is especially useful at inboard design stations, where the shock is generally further aft on the wing but it is not practical to try to extend laminar flow to that location. An option also exists to adjust the target shock location toward the current shock location as the design progresses. This option has proven to be very stable while providing reasonable shock locations. In addition, as shown in figure 10, the decoupling of the 2 locations allows a mild adverse pressure gradient to be used aft of X3 to reduce the shock strength as well as ensure transition before the shock is reached. Initial results indicate that the shock Mach numbers were successfully reduced.

While the primary focus of the SSNLF constraint is to prescribe a pressure distribution that will support natural laminar flow while minimizing any wave drag penalty, the constraint has also been modified to adjust the loading behind the shock to give a desired pitching moment coefficient while maintaining adequate airfoil thickness in the cove region near the trailing edge. The current version of SSNLF uses the equation

$$c_m = -0.32 * c_l^2 \quad (2)$$

where c_m and c_l represent the section pitching moment and lift coefficients, respectively, at each design station. This equation was calibrated using the baseline CRM values, but adjusted to provide slightly more aft loading at inboard stations. The constraint seems to produce reasonable target pressures over the aft end of the airfoils and the increased aft loading inboard gave reduced shock strengths at those design stations.

As with the CF LASTRAC results in the previous section, the effect of using the various input options will be examined using the pressures and geometry for station 6 from the CRM NLF wing. The standard β=0 TS results using LST for the baseline and design airfoils are shown in figures 18a and 18b, respectively. At this station, the baseline wing has a moderate adverse pressure gradient (see figure 11) that causes rapid TS N-factor growth, resulting in a transition location near x/c = 0.25 for the critical N-factor of 10. The design N-factors rise fairly quickly to an N-factor of 5, then grow at a nearly linear rate until the critical N-factor is reached at the desired transition location of x/c = 0.6. The linear growth in the midchord region is intended to provide a gradual shift in the transition front at off-design conditions.

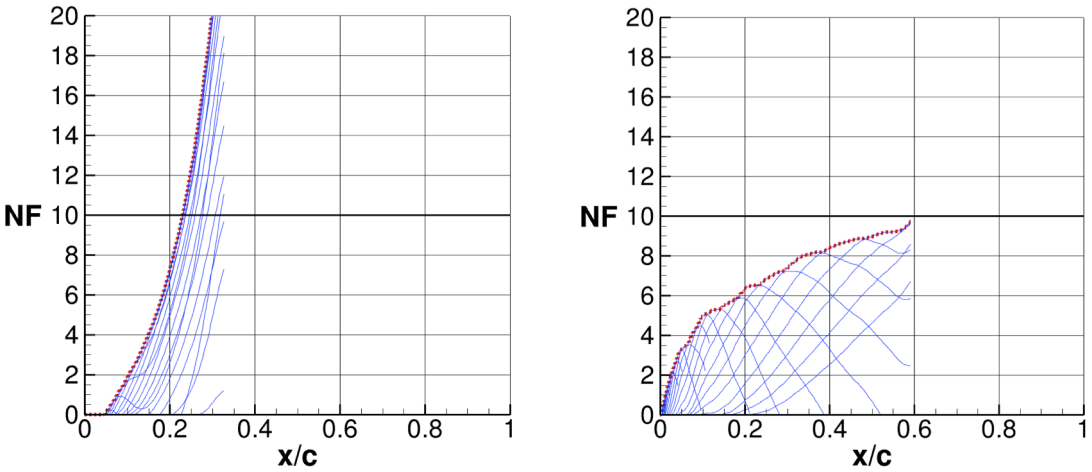

a) Baseline. **b) Design.**

Figure 18. Comparison of TS N-factors for baseline and design at station 6.

In contrast to the CF compressibility effects being small, for TS, there is a significant damping effect on the N-factor growth (figures 19a and 19b). In previous unpublished work with researchers from the German aerospace organization (DLR), it was found that the Karman-Tsien scaling factor that is commonly used to scale between incompressible and compressible pressure distributions could also be applied to TS N-factor distributions as they are largely driven by pressure gradients. Figure 19c shows that the scaled incompressible N-factor envelope is close to the compressible envelope, lending credence to the results.

The effects of streamwise curvature on TS were examined next. Contrary to the results for CF, curvature had essentially no effect on TS N-factor growth, as the area where the TS growth is occurring has low curvature compared to the leading-edge region (see figures 20a and 20b). Both the curvature and compressibility options do not add any significant time to the analysis and would seem to represent a better modeling of the physics, but it would require that they also be used in the determination of critical N-factors.

An attempt was made to evaluate the effects of running in PSE mode vs LST for TS, with the results shown in Figure 21. The lack of significant early N-factor growth raises some questions about the validity of the PSE result, but levels near midchord are similar, with the PSE envelope approaching the critical NF value of 10 with a slightly steeper slope than LST. This would appear to move the transition location slightly forward relative to the LST value and would thus be more conservative. However, this single PSE case required just under 12 hours to run, making it unrealistic in the design environment.

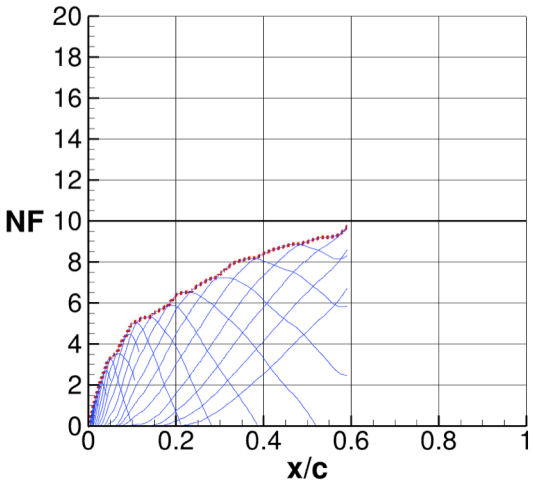

a) Baseline.

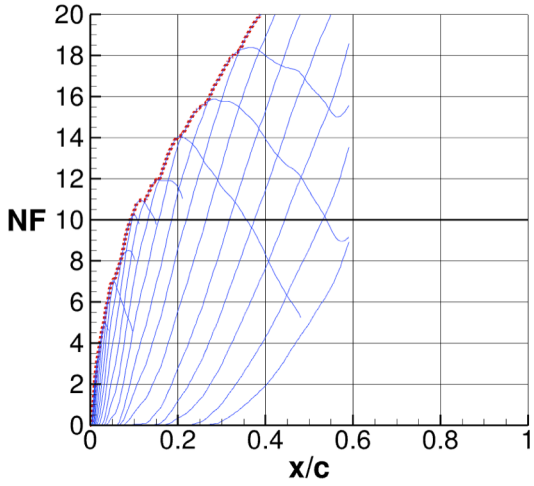

b) Design.

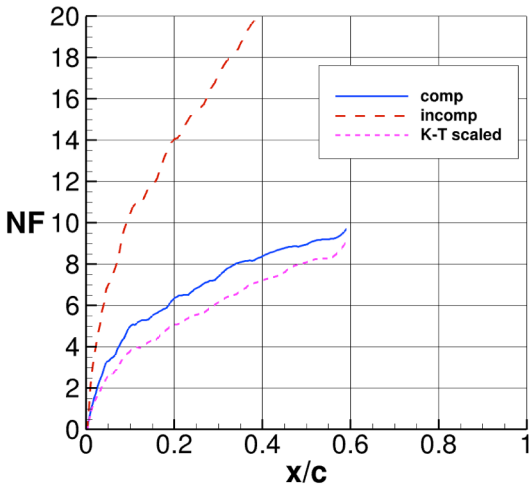

c) Karmen-Tsien scaling applied to incompressible TS N-factor envelope.

Figure 19. Effect of incompressibility on TS N-factors.

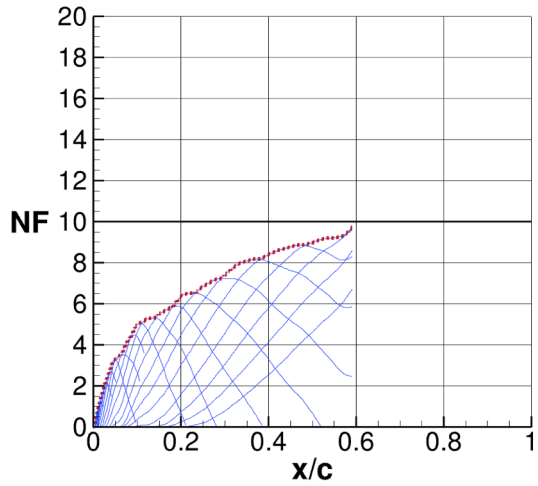

a) No curvature.

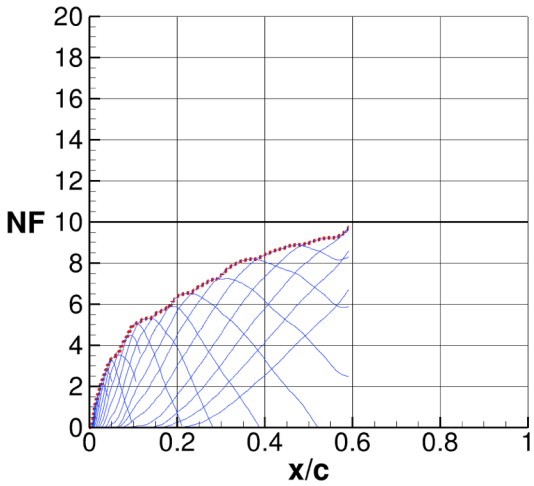

b) Curvature.

Figure 20. Effect of curvature on TS N-factor of design at station 6.

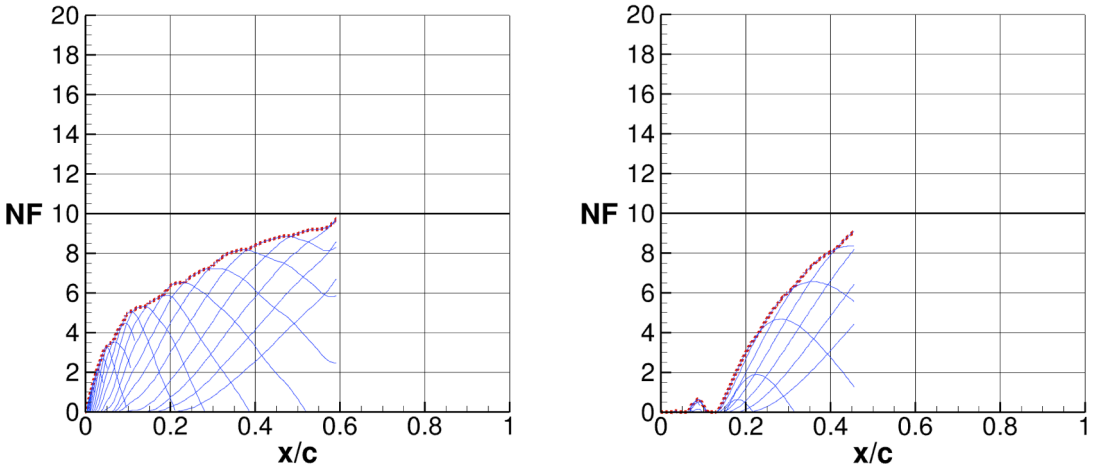

a) LST. b) PSE.

Figure 21. Effect of PSE on TS N-factors.

A much more efficient alternative would be the MATTC code. This code has given reasonable estimates of the TS N-factor envelope, especially when calibrated to a specific case. Figure 22a indicates the quality of matching between MATTC and LASTRAC when the algorithm coefficients are calibrated. MATTC was calibrated using all of the design stations for the CRM NLF wing and comparisons are made with LASTRAC results for each station. The results are shown in figure 22b in terms of the predicted transition fronts for 3 critical N-factors, with the MATTC results shown as lines and the LASTRAC predictions indicated by symbols. The agreement between the 2 methods is generally good and indicates that MATTC could be used in the design loop with reasonable accuracy. To obtain a calibration prior to a design, the initial target pressures could probably be used as representative of the final design pressures. Additional calibrations could also be performed at intermediate stages if required.

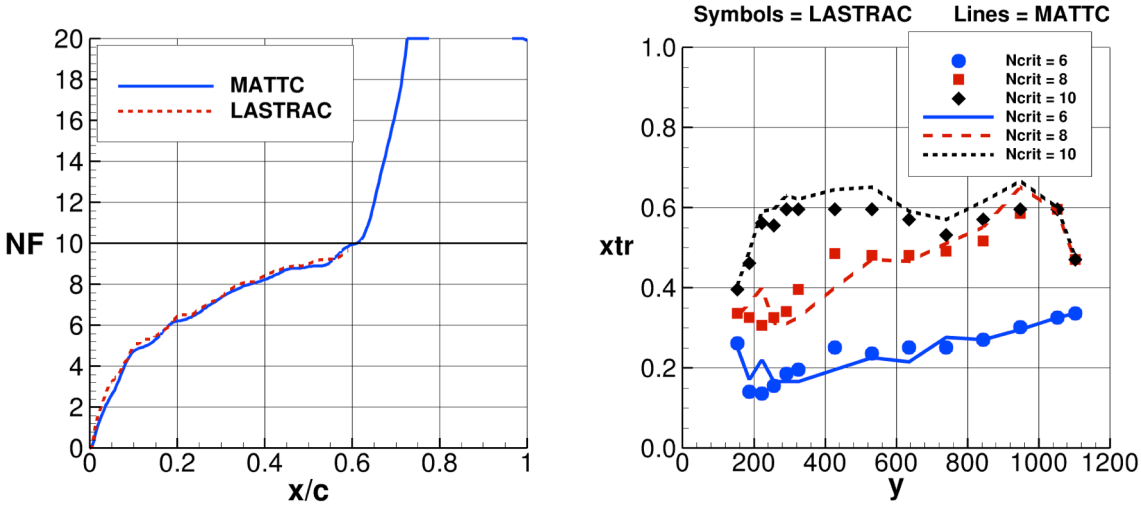

a) Station 6. b) Transition front locations.

Figure 22. Comparison of LASTRAC and MATTC predictions for TS N-factors.

Based on comments in Arnal[9] and recommendations from NASA stability analysis experts, our transonic design work to date was done without considering OTS and TCF. In the supersonic work, an equation defining dominant frequency-β pairs was developed, with an automated process for checking other combinations for higher N-factor levels. As this equation did not exist for transonic flow, we defined a test matrix of 300 frequency-β pairs to evaluate

our assumption of the TS with β = 0 and stationary CF being at least representative of the dominant growth curves. The N-factor growth curves for each pair are shown in figure 23a, with the thin blue and red curves corresponding to positive and negative values of β, respectively, and the red dashed curve being the envelope or crest line over all of the curves. In figure 23b, the crest line over these frequency-β search (FBS) curves is plotted in red, along with the previous envelopes from the TS (green) and CF (blue) calculations. As can be seen, the TCF peak at the front of the FBS curve is only slightly higher than our standard CF. As the critical N-factor quoted for TCF in flight is typically higher than our limit of 10, this suggests that our use of standard CF is probably reasonable. However, the OTS portion of the FBS curve is about 40% higher than our standard TS curve. This result was surprising in view of our typical edge Mach number values of 1.25 being well below the 1.5 value where we understood OTS would become dominant. Further evaluation of these results is underway, including the development of a dominant frequency-β pair equation for transonic flow. In addition, it is possible that MATTC could be calibrated against OTS results instead of the standard TS. Finally, if the critical N-factor for TS was extracted using standard TS, then to be consistent we would still want to use the same analysis.

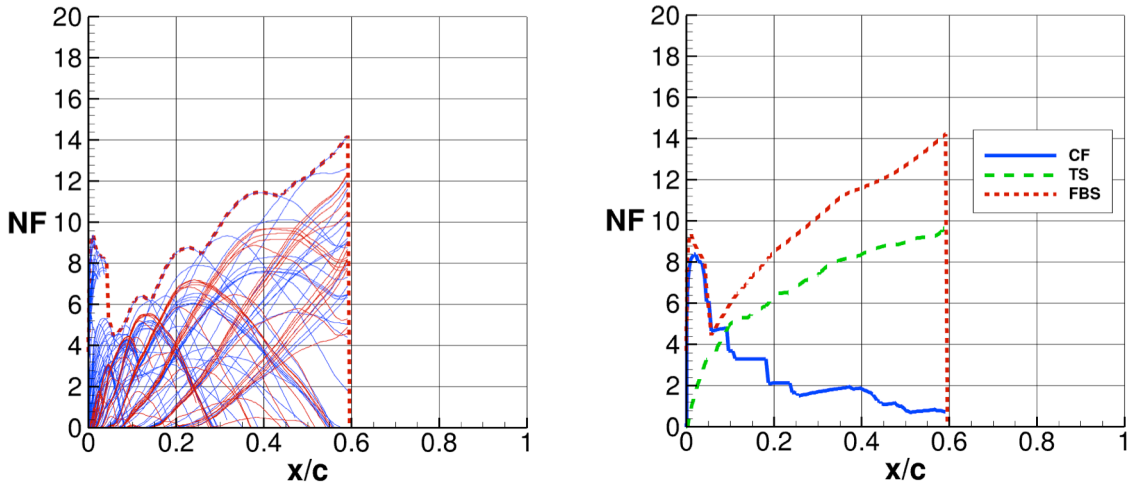

a) FBS individual curves. **b) TS, CF, and FBS crests.**

Figure 23. Results from nonzero frequency-β pairs study.

As mentioned earlier, our analysis has used a fixed-β approach rather than an envelope method, at least in part because there is not a direct option for it in LASTRAC. Some previous research by Arnal[9] and Ueda[18] suggests that the envelope method is less consistent than fixed-β and can give unphysically high critical NF values at transition. A work around to use LASTRAC in this mode has been proposed and may be further developed to at least allow the assessment of the differences. Another possible approach to predicting transition is the use of one of the emerging models built directly into the flow solver such as the ones by Coder[19] and Langtry[20], with the latter of these attempting to account for CF. Two capabilities that would be needed for our design method are the inclusion of CF effects and some form of calibration to take into account the different critical N-factor levels in tunnels versus flight.

In summary, relative to transition prediction as part of a practical NLF design method, it would appear that LST analysis is not fast enough to be included within the design loop, but is sufficiently accurate and efficient to be used as a final check on the design. The MATTC code is very efficient and, if calibrated using LASTRAC, may be practical to include within the design module itself as a driver in defining target pressures or in adjusting transition location in an off-design analysis. At this stage, it would appear that the time required for PSE analysis is prohibitive and the benefits in accuracy are not clear. Relative to the options available in LST, none had a significant impact on analysis time, but some had a large effect on the NF growth (e.g., compressibility for TS, curvature for CF). It would seem that using the options that best account for the physics would be the reasonable choice, but ultimately the critical NF levels would have to be determined using the same options. In the planned wind tunnel test of the CRM NLF model, multiple LST options will be used in extracting critical N-factors to allow these evaluations.

D. Design Process

In general, the current laminar flow design process differs little from the design of a turbulent wing case. The previous CDISC turbulent design rule of thumb of 20 design cycles with each cycle run for 1/20th of the number of

flow iterations needed for the initial converged solution still holds, producing a good indication of the success of the set of constraints selected. Final convergence in both cases (laminar and turbulent) is typically achieved in 10 to 20 more design cycles. Two new features in the design loop are a configuration angle-of-attack adjuster to match the desired total lift and a code (LAMEST) that predicts the amount of laminar flow to prescribe in the flow solution. The lift adjustment feature has been more stable than the built-in lift matching option in USM3D and provides better results than a fixed-alpha design that is then analyzed at the correct lift.

The current strategy for specifying the extent of laminar flow in USM3D uses the LAMEST code to read the desired transition location from the CDISC target input file and then adjust it forward if a value of the skin friction coefficient less than 0.0001 is encountered ahead of this location. An additional forward movement of 0.1c from the target transition location is included to help prevent flow code divergence during the early design cycles when shocks could potentially move into the laminar region. The overall assumption with this approach is that the final design will match the target pressures with sufficient accuracy to avoid the CF and AL transition modes that are more severe. Experience thus far indicates that this is a reasonable assumption and saves considerable time compared with running the LASTRAC code during each design cycle, even if the LST option is used.

A couple of issues related to grid quality were encountered in the early stages of the design of the CRM wind tunnel model, both related to the unstructured surface grid consisting of triangles with uneven spacing. For nearly all of the design stations, the pressure and geometry information is extracted from the grid and flow solution by passing a streamwise cutting plane through the wing surface, then interpolating the results to a consistent set of x/c locations at every station. The CDISC code then modifies the coordinates at these locations and the design process distributes these changes back into the surface grid using linear interpolation between stations. The extraction and interpolation process can create small curvature variations that can get amplified during design, especially for cases where design stations are closely spaced in the spanwise direction. This effect was most noticeable near the wing root, where several new stations were added for use with the LEMOD constraint to address attachment line contamination. Although the resulting pressure oscillations would probably not be of consequence in a turbulent design, they were large enough to cause early termination of the boundary layer calculation at some design stations.

In order to address this issue, several new codes have been developed. The first one (GPA) moves the surface grid points nearest each design station so that they fall on that spanwise location of the design station. While this step helps immensely in reducing spurious curvature variations, some still occur. A second code (SMOGPA) has just been developed to post-process the grid from GPA to give the points on the design station a smoother distribution in arc length along the surface. The end result of this process is to locally simulate a structured grid while retaining the advantage of unstructured grid generation for complex configurations. These two codes are applied to the baseline grid before starting the design process. In addition, a new version of the code that distributes the design changes between stations after each cycle has been developed. It uses a nonlinear lofting of the changes between stations that should further improve the smoothness of the final wing.

Figure 23 gives an indication of the smoothness of the design pressures and how well the target pressures are matched at inboard, midwing and outboard design stations for the current design. In general, the agreement between design and target pressures is good, though the shock is forward of the target location at the midwing station (figure 23b). This case was run without the shock location adjustment feature turned on. Although the midwing station did not benefit from the mild adverse gradient in the target pressures ahead of the shock, it did achieve the full amount of laminar flow desired.

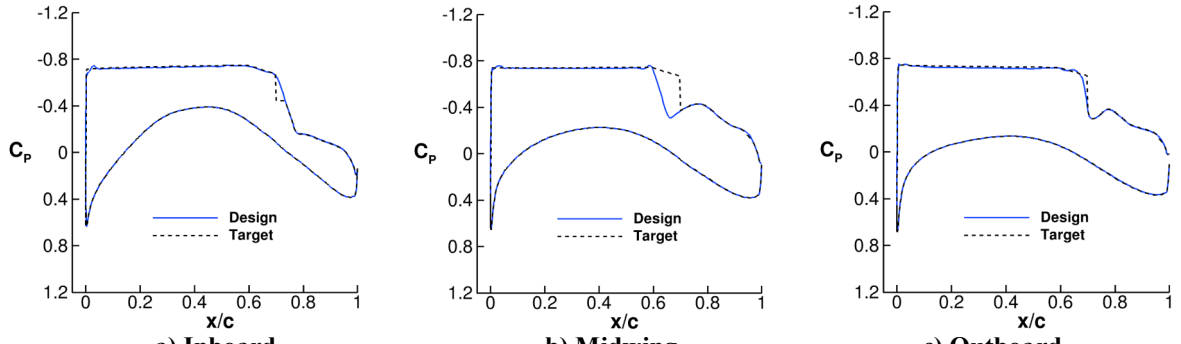

a) Inboard. **b) Midwing.** **c) Outboard.**

Figure 23. Sample design pressures from the CRM NLF design.

The general process improvements listed above came out of our experience on the CRM NLF wing design. As we began to apply the NLF design method to other configurations and components, some useful modifications to the SSNLF constraint itself became apparent; specifically, the options to apply just the CF or TS control pieces of the constraint. For example, over the inboard portion of a hybrid wing body, it may be possible to maintain a laminar attachment line and small region of laminar flow near the leading edge, but features such as windscreens or the need to maintain internal volume shape for passengers or cargo would preclude the midchord modifications required to control TS growth. In other cases, the wing may already have a pressure distribution that would limit TS growth, but does not control CF adequately. The new CF-only option utilizes the pressure architecture up to X2, then blends into the current distribution just aft of that point. A simple 2-D example of this option is shown in figure 24, where X1 is 0.001 and X2 is 0.05, and all of the changes are restricted to be ahead of x/c = 0.1 (see figure 24b). As shown in figure 24a, the rapid acceleration followed by a short distance of zero pressure gradient was achieved with minimal impact aft of x/c = 0.1. Designing using such a limit region is usually very difficult and this may have just been a fortuitous result, but it does suggest that the CF-only option may be useful in some cases.

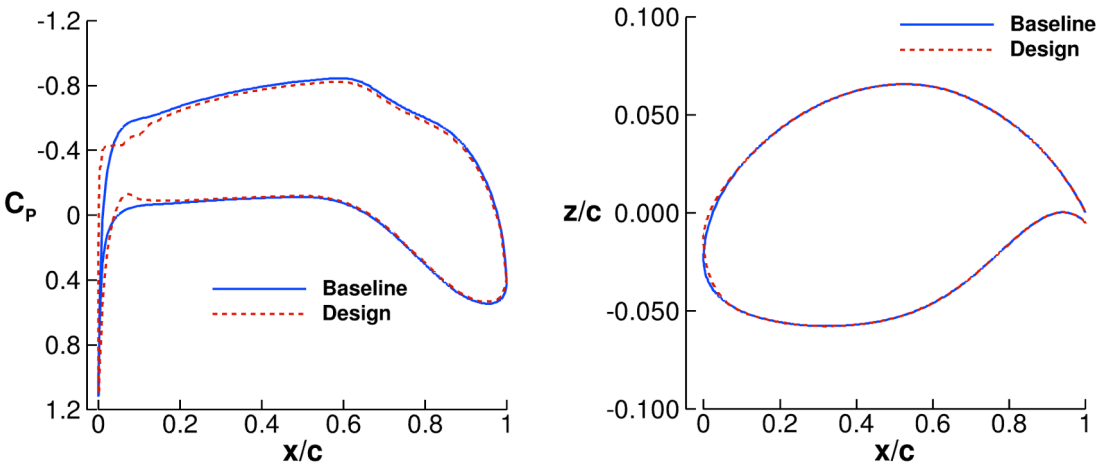

a) Pressure distribution. **b) Geometry.**

Figure 24. Results from CF-only design limited to airfoil leading-edge region.

The other new option, applying only the portion of SSNLF between X2 and X3 (see figure 9) for TS control, was developed as we began to explore NLF nacelle design. It is assumed that at cruise conditions that there is no significant CF growth or attachment line issues, so the only mode needing to be controlled is TS. In addition, in order to retain inlet flow characteristics, the design is typically limited to the outer nacelle surface. It should be noted that CDISC is also effective for internal flow design and that ideally both surfaces could be designed at the same time. To test this option, a design case was set up for the CRM nacelle (see figure 25), with design stations at azimuthal angles of 0, 90, 180 and 270 degrees (measured clockwise from the top when viewed from behind). The flow solver, CART3D, was run at a Mach number of 0.85 and an angle of attack of 2 degrees. As mentioned earlier, CART3D is inviscid, but it is assumed that nacelle pressure distributions are not significantly affected by the boundary layer at cruise conditions. A constraint on the thickness of the nacelle "airfoils" is included to limit the growth of the maximum nacelle radius to minimize any increases in wave or boat-tail drag.

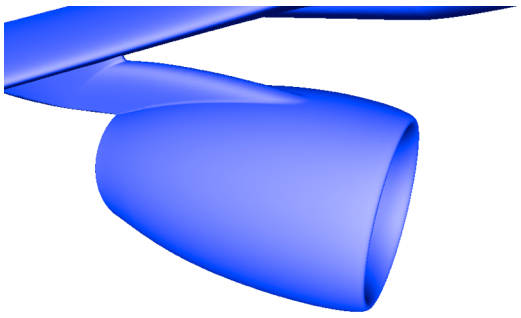

Figure 25. Shaded view of CRM nacelle.

For this design, the TS-only option in the SSNLF constraint in CDISC was further modified to include MATTC for determining the value of UDF required for the target pressure to reach the desired transition location of x/c = 0.5

at a critical NF of 10. The MATTC coefficients used in the design were calibrated against LASTRAC results for the initial target pressures from the stations at 90, 180 and 270 degrees (no direct laminar flow design was applied at 0 degrees due to the presence of the pylon, though the pressure levels there were limited to a local Mach number of 1.1). The design was run for 30 cycles and resulting pressure distributions are shown for the 3 main design stations in figure 26. CDISC was able to eliminate the leading-edge peak and match the nearly-flat NLF target pressures ahead of x/c = 0.5 fairly well, though there are some small oscillations in the design pressures. The reason for the collapse of the pressure architecture near the leading edge at 270 degrees is not clear, and for a later design in USM3D using the same target set up (not shown), this feature was not present to the same extent. The expansion immediately before the shock near x/c=0.6 at 90 and 180 degrees is not desirable and suggests a further modification to the TS-only option for future designs to limit this rise in shock Mach number.

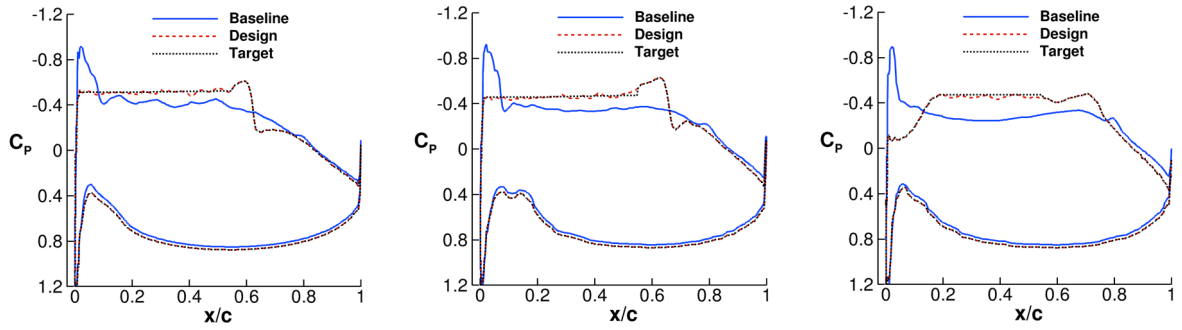

a) 90 degrees. **b) 180 degrees.** **c) 270 degrees.**

Figure 26. Design pressures from the CRM NLF nacelle design.

The resulting NF growth envelopes are shown in figure 27 for both MATTC and LASTRAC, with results for the design pressures on the left side of the figure and results for the target pressures on the right. At 90 and 180 degrees, the NF envelopes from both analysis methods for the target pressures are similar and provide the desired transition location of x/c = 0.5 at the critical NF of 10 (figures 27b and 27d). For the station at 270 degrees (figure 27f), the agreement between the 2 methods is not as good, though the LASTRAC prediction does match the desired extent of NLF. At this station, MATTC did not adjust the UDF parameter from the initial value of zero because the transition location was already at the desired value due to the strong favorable gradient at the front of the station suppressing early TS growth. The SSNLF constraint has now been modified to drive the transition location explicitly to the target value, adding an adverse pressure gradient if needed. Even without this change, however, the transition locations predicted by the 2 methods were within 0.1c of each other.

For the design pressures (figures 27a, 27c, and 27e), correlation between MATTC and LASTRAC is not as good as desired, with only the station at 90 degrees achieving a decent match. Apparently, the oscillations in the design pressure distributions, especially near the leading edge, are large enough to trigger significant early TS growth in LASTRAC that is not getting picked up by MATTC to the same degree. The wing design pressures shown in figure 23 did not seem to have this problem, so it is thought that the oscillations are probably more related to gridding issues. The grid has triangular faces that are stretched in the circumferential direction near the leading edge and is fairly coarse in general compared to the criteria used for NLF wing grids. Also, the nacelle has much more traverse curvature than a wing, which tends to increase the tessellation effect in the computation as well as in interpolating the design changes back into the grid. Finally, the grid used for this test study did not utilize the GPA and SMOGPA processes to improve the smoothness of the design on triangulated grids. Further work this summer will address these issues. It is also possible that the restriction of designing only the outer surface of the nacelle could introduce some flow oscillations near the leading edge independent of the grid quality.

In summary, based on the reasonable agreement between the two analysis methods for the target pressures, MATTC shows promise as a stability analysis method within the design loop as part of the TS-only NLF design option in CDISC. If the target pressures had been better matched by the CDISC design for this nacelle case, a second calibration of MATTC using the final LASTRAC results perhaps could give a more accurate result with further design cycles.

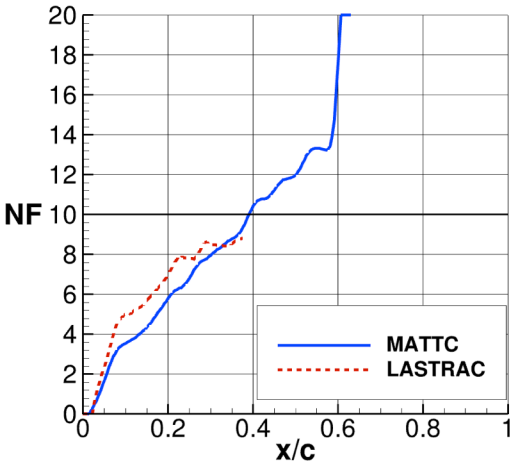

a) Analysis pressures at 90 degrees.

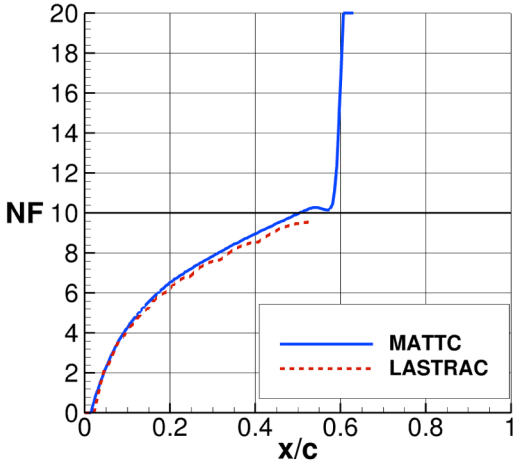

b) Target pressures at 90 degrees.

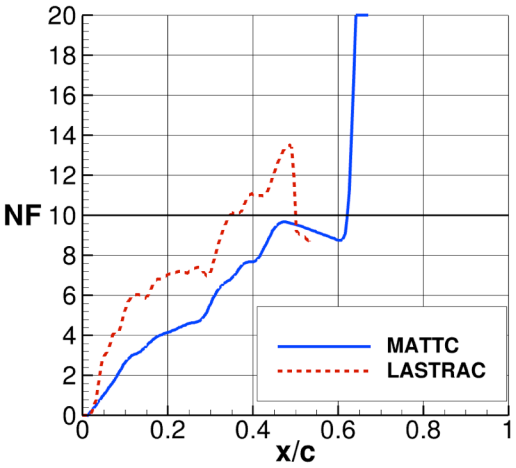

c) Analysis pressures at 180 degrees.

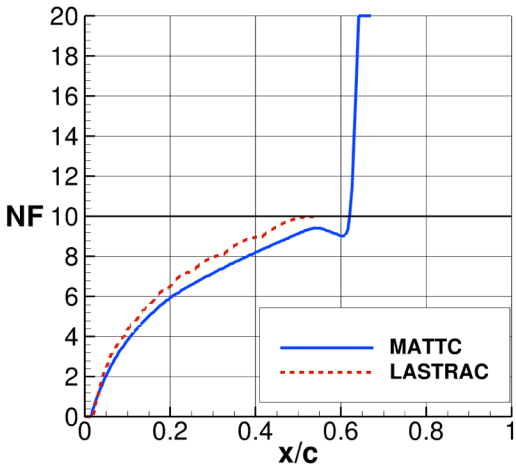

d) Target pressures at 180 degrees.

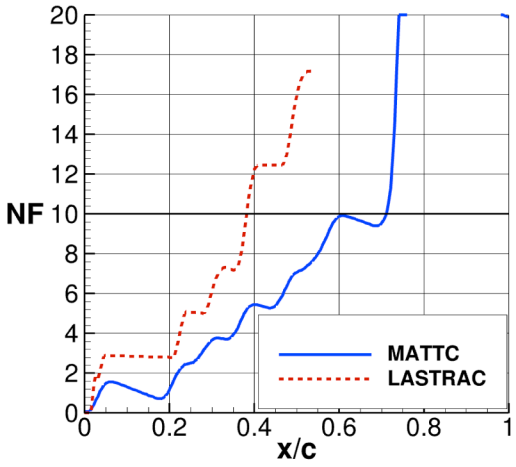

e) Analysis pressures at 270 degrees.

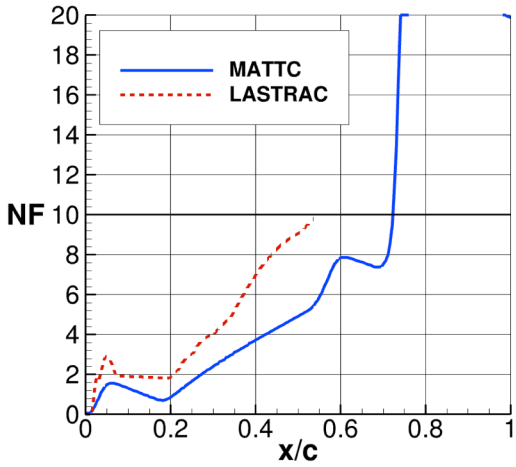

f) Target pressures at 270 degrees.

Figure 27. N-factor growth envelopes from TS-only design applied to the CRM nacelle.

IV. Concluding Remarks

Significant progress has been made toward evolving the initial NLF design process reported on previously by the authors into a practical design system. New features have been added to the CDISC design module that address attachment line contamination and transition. For TS and CF modes of transition, a number of options in the LASTRAC stability analysis code were exercised to evaluate our original choice of running LST with compressibility but no curvature effects included. For TS, compressibility had a very large impact, with the incompressible NF levels more than a factor of 2 higher than our standard compressible analysis. The effect of curvature was negligible for TS, but had a large suppressing effect on CF. Unlike TS, compressibility had little effect on CF. For both TS and CF, using PSE analysis instead of LST had little effect on the levels, but required so much run time that it was deemed prohibitive in the context of an NLF design system. Finally, we also evaluated nonzero frequency-β pairs for OTS and TCF for our transonic case in a similar fashion to our standard approach for supersonic design. The effect of this on the maximum CF peak height near the leading edge was only a slight increase for TCF, but the OTS levels were higher by about 40% relative to our standard TS.

While noting all of the above effects on TS and CF for the various options, the key point appears to be consistency with the methods or options used in determining critical NF levels from experimental data. While it would seem reasonable to include as much flow physics as possible in the computation, especially as the various LST options did not noticeably affect the run time, the higher level of physics could give a false indication of design success or failure if it is not consistent with the critical level extraction process. For our upcoming CRM NLF model test in the NTF, the plan is to use all options in LST in estimating critical NF levels for the tunnel.

Finally, as we began to apply our NLF design method to other configurations and components, it became apparent that it would be useful to not overprescribe the NLF target pressure distribution, so options were developed to apply only the TS or CF control as needed. An initial example of each is provided, with the TS-only nacelle design utilizing the rapid low-fidelity MATTC method for transition prediction in the NLF target definition in the design loop. While both results are promising, additional areas for improvement have been identified and are being pursued.

Acknowledgments

This research is funded by the NASA Advanced Air Transport Technology Project in the Advanced Air Vehicles Program and the Flight Demonstration Capabilities Project within the Integrated Aviation Systems Program. The authors would like to thank Dr. Ponnampalam Balakumar, Dr. Chau-Lyan Chang, Dr. Meelan Choudhari, and Dr. Lewis Owens of the NASA Langley Research Center for their many helpful discussions on the theory and application of boundary layer stability computations.

References

[1] Crouch, J., "Boundary-Layer Transition Prediction for Laminar Flow Control (Invited)", 45th AIAA Fluid Dynamics Conference, AIAA AVIATION Forum, AIAA 2015-2472, 2015.

[2] Fujino, M., "Design and Development of the HondaJet", AIAA International Air and Space Symposium and Exposition: The Next 100 Years, AIAA 2003-2530, July 2003.

[3] Campbell, R.L., and Lynde, M.N., "Natural Laminar Flow Design for Wings with Moderate Sweep", 34th AIAA Applied Aerodynamic Conference, AIAA AVIATION Forum, AIAA 2016-4326, June 2016.

[4] Lynde, M.N. and Campbell, R.L., "Expanding the Natural Laminar Flow Boundary for Supersonic Transports", 34th AIAA Applied Aerodynamic Conference, AIAA AVIATION Forum, AIAA 2016-4327, June 2016.

[5] Vassberg, J.C. and Rivers, S.M., "Development of a Common Research Model for Applied CFD Validation", AIAA 2008-6919, August 2008.

[6] Frink, N.T., Pirzadeh, S.Z., Parikh, P.C., Pandya, M.J., and Bhat, M.K., "The NASA Tetrahedral Unstructured Software System," The Aeronautical Journal, Vol. 104, No. 1040, October 2000, pp.491-499.

[7] Aftosmis, M. J., Berger, M. J., and Adomavicius, G.: "A Parallel Multilevel Method for Adaptively Refined Cartesian Grids with Embedded Boundaries", AIAA 2000–808, January 2000.

[8] Chang, C.-L., "The Langley Stability and Transition Analysis Code (LASTRAC): LST, Linear and Nonlinear PSE for 2-D, Axisymmetric, and Infinite Swept Wing Boundary Layers," AIAA 2003-0974, 2003.

[9] Arnal, D; Casalis, G., and Houdeville, R.: "Practical Transition Prediction Methods: Subsonic and Transonic Flows", RTO-EN-AVT-151, pp. 7.8 – 7.16., June 2008.

[10] Wie, Y.-S., "BLSTA: A Boundary Layer Code for Stability Analysis," NASA CR 4481, 1992.

[11] Campbell, Richard L.; Campbell, Matthew L.; and Streit, Thomas: "Progress Toward Efficient Laminar Flow Analysis and Design", AIAA 2011-3527, June 2011.

[12] Campbell, R.L., "Efficient Viscous Design of Realistic Aircraft Configurations," AIAA-98-2539, June 1998.

[13] Poll, D. I. A., "Some Observations of the Transition Process on the Windward Face of a Long Yawed Cylinder," J. Fluid Mech., Vol. 150, 1985, pp. 329-356.

[14] Gaster, M.: On the Flow Along Swept Leading Edges. Aeronaut. Q., vol. XVIII, pt. 2, pp. 165-184, 1967.
[15] Joslin, Ronald D.: "Overview of Laminar Flow Control", NASA/TP-1998-208705, October 1998.
[16] Alderman, James; Rolston, Stephan; Gaster, Michael; and Atkin, Chris: "A method of Reducing the Drag of Transport Wings", AIAA 2016-3115, June 2016.
[17] Malik, Mujeeb; Liao, Wei; Lee-Rausch, Elizabeth; Li, Fei; Choudhari, Meelan; and Chang, Chau-Lyan: Computational "Analysis of the G-III Laminar Flow Glove", AIAA 2011-3525, June 2011.
[18] Ueda, Yoshine; Yoshida, Kenji; Matsushima, Kisa; Ishikawa, Hiroaki: "Supersonic Natural-Laminar-Flow Wing-Design Concept at High-Reynolds-Number Conditions", AIAA Journal, Vol. 52, No. 6, June 2014.
[19] Coder, James G.: "Enhancement of the Amplification Factor Transport Transition Modeling Framework", AIAA 2017-1709, January 2017.
[20] Langtry, Robin B.; Sengupta, Kaustav; Yeh, David T.; and Dorgan, Andrew J.: "Extending the γ-$Re_{\theta t}$ Local Correlation based Transition Model for Crossflow Effects", AIAA 2015-2474, June 2015.